Received: 6 January 2025 | Accepted: 29 May 2025

DOI: 10.1002/agg2.70160

Agrosystems, Geosciences & Environment OPEN ACCESS

ORIGINAL ARTICLE

Geosciences

Estimating leaf phosphorus concentration in rice by combining vegetation indices, texture features, and water indices from UAV multispectral imagery

Canh Van Le | **Lan Thi Pham**

Faculty of Geomatics and Land Administration, Hanoi University of Mining and Geology, Ha Noi, Vietnam

Correspondence
Lan Thi Pham, Faculty of Geomatics and Land Administration, Hanoi University of Mining and Geology, 18 pho Vien, Duc Thang, Bac Tu Liem, Ha Noi, Vietnam.
Email: phamthilan@humg.edu.vn

Assigned to Associate Editor Phuong Dao.

Abstract

Leaf phosphorus (P) concentration is a key factor that reflects the growth of rice *(Oryza sativa)*, affecting both the quality and productivity of the crop. The estimation of leaf P concentration using unmanned aerial vehicle (UAV) remote sensing plays a pivotal role in fertilization management, monitoring rice growth, and advancing precision agriculture strategies. This study aimed to integrate vegetation indices (VIs), texture features (TFs) indices, and water indices (WIs) obtained from UAV multispectral images to estimate leaf P concentration in rice using the multi-criteria evaluation (MCE) model with analytical hierarchy process–based weights. The MCE method was employed to integrate the 16 VIs, eight TFs, and two WIs with four scenarios (S1, S2, S3, and S4) to evaluate their contributions to estimating the rice leaf P concentration. The S1 integrates the normalized difference vegetation index (NDVI), the modified chlorophyll absorption in reflectance index (MCARI), and the mean (MEA). The S2 extends S1 by incorporating the normalized difference water index (NDWI), while S3 combines the indices from S1 with NIR shoulder region index (NSRI). Finally, S4 integrates NDVI, MCARI, MEA, NDWI, and NSRI. The S4, which integrates all VIs, TFs, and WIs, provides the highest accuracy in estimating leaf P concentration with root mean square error values of 0.035. The research findings indicate that leaf P concentration differs between the two rice varieties, TBR225 and J02. The J02 variety exhibits a higher leaf P concentration than the TBR225 variety, as it is more efficient in P synthesis. The results of this study provide an effective foundation for developing solutions in rice nutrition management, with a focus on advancing precision agriculture.

Abbreviations: AHP, analytical hierarchy process; DVI, difference vegetation index; GNSS, global navigation satellite system; MCARI, modified chlorophyll absorption in reflectance index; MCE, multi-criteria evaluation; NDVI, normalized difference vegetation index; NDWI, normalized difference water index; NIR, near-infrared; NSRI, NIR shoulder region index; P4M, DJI Phantom 4 Multispectral; PCA, principal component analysis; RE, red edge; RMSE, root mean square error; RTK, real-time kinematic; TFs, texture features; UAV, unmanned aerial vehicle; VIs, vegetation indices; WIs, water indices.

Plain Language Summary

The amount of phosphorus in rice leaves is an important indicator of rice growth, influencing both crop quality and yield. Using drones (unmanned aerial vehicles [UAVs]) to estimate leaf phosphorus concentration helps manage fertilizer use, monitor plant health, and improve precision farming techniques. This study combined three types of data—vegetation indices, texture features, and water indices—from UAV multispectral images to estimate leaf phosphorus concentration using a multicriteria evaluation model with analytical hierarchy process–based weighting. The results show that leaf phosphorus concentration varies between two rice varieties, TBR225 and J02. The J02 variety has higher leaf phosphorus concentration than the TBR225 variety because it processes phosphorus more efficiently. These findings help improve rice nutrition management and support precision agriculture advancements.

1 | INTRODUCTION

Rice *(Oryza sativa)* is the primary staple food and the most essential commodity in daily life in Vietnam. Rice yield is significantly influenced by balanced fertilizer application, with P playing a critical role (Guo et al., 2024; Irfan et al., 2020). Moreover, P plays a critical role in influencing nitrogen (N) uptake during different growth stages of rice plants. Phosphorus deficiency reduces N concentration in leaves during the mid-tillering stage but increases N concentration at the early heading stage when the same amount of N fertilizer is applied (Peng et al., 2015). Phosphorus plays a vital role in nearly all energy-dependent biological processes in plants, including photosynthesis, respiration, membrane transport, and the synthesis of cellular components (Tisdale & Nelson, 1985).

There are several methods for estimating leaf P concentration that can be categorized into traditional and remote sensing techniques. Although traditional methods are accurate, they are costly, time consuming, laborious, and destructive (Siedliska et al., 2021). Additionally, these methods offer limited insights and are not suitable for monitoring the spatial and temporal variations of biochemical component contents across large areas (Zhai et al., 2013). In contrast, remote sensing can directly monitor crop conditions, allowing for timely interventions without the need for destructive sampling (Pinter et al., 2003; Ryu et al., 2020). Remote sensing–based estimation of leaf P concentration plays a vital role in enhancing fertilization management, tracking crop growth, and promoting precision agriculture strategies (Y. Zhang et al., 2023). The spectral reflectance of crop leaves has been shown to correlate with their P status (Lu et al., 2020; Magalhães et al., 2022; Mahajan et al., 2016; Pimstein et al., 2011). Therefore, establishing a diagnostic model for leaf P concentration using remote sensing technology is crucial for precise P fertilizer management.

Remote sensing technology is a critical component of precision agriculture and is increasingly being adopted by scientists, engineers, and large-scale crop producers (Liaghat & Balasundram, 2010). Remote sensing data can be collected through a range of platforms, including ground-based, manned aircraft, satellite, and unmanned aerial vehicle (UAV) to assess precision agriculture (Velusamy et al., 2021). The varying spatial and temporal resolution of satellite-captured images makes them a preferred option for wide-area and field-scale agricultural monitoring (Faustin, 2024). On the other hand, UAVs offer flexibility for a wide range of applications and provide effective solutions to challenges encountered by other remote sensing platforms, as they are cost-effective, easily deployable in various locations, and capable of capturing real-time spatial images (Delavarpour et al., 2021). The UAV have undergone rapid advancements since the late 20th century, with significant progress in their application for monitoring crop parameters, attributed to their exceptional temporal and spatial resolution capabilities (Ban et al., 2022; Sishodia et al., 2020; J. Zhang et al., 2022). The UAV-based remote sensing technology has been extensively employed to derive the physical and chemical properties of rice, emerging as a key approach for remotely collecting data at the plot level in rice fields (Dumitru, 2023; Rudoy et al., 2020). UAVs have been successfully employed in monitoring nutrient levels in crops in general and rice plants in particular (Zheng et al., 2018).

Spectral reflectance data from bands such as green, red, red edge (RE), and near-infrared (NIR), combined with vegetation indices (VIs) like the normalized difference vegetation index (NDVI), ratio vegetation index, medium resolution imaging spectrometer terrestrial chlorophyll index, difference vegetation index (DVI), and green normalized difference vegetation index, serve as fundamental tools for investigating agricultural parameters (Y. Liu et al., 2021; S. Zhang et al.,

2019) including leaf N, P, and potassium (K) concentrations. Among these nutrient parameters, leaf N concentration (Colorado et al., 2020; Khose & Mailapalli, 2024; S. Xu et al., 2023) and leaf K concentration (Lu et al., 2020; Yu et al., 2023) have been widely studied. However, the estimation of leaf P concentration using UAV imagery remains significantly constrained. This limitation arises from the low sensitivity of the spectral bands in UAV multispectral imagery to leaf P concentration. Additionally, leaf P concentration is indirectly manifested through the plant's metabolic and energy processes, which are reflected in leaf water content and structure. Therefore, this study expands a new solution to identify the relationship between leaf P concentration and UAV-derived spectral data through water-related factors, VIs, and texture features (TFs).

During plant growth, changes in P levels lead to alterations in leaf color (Hoque et al., 2010), chlorophyll content (Tairo & Ndakidemi, 2013), water content (S. Jiang et al., 2023), and canopy TFs (Barbosa et al., 2014; J. Zhang et al., 2022). Moreover, canopy texture is a crucial component of UAV imagery, where variations in structure in UAV imagery reflect differences in leaf P levels.

Apart from its influence on spectral reflectance and leaf structure, P content also affects the water content of plant leaves. Phosphorus deficiency significantly impacts the relative water content retained by leaves (Oukaltouma et al., 2020). The positive relationship between leaf P concentration and water content has been observed in cotton (*Gossypium hirsutum*) leaves (Singh et al., 2006). Spectral regions ranging from the visible spectrum to the short wave infrared (SWIR) are crucial for identifying leaf P concentration (Li et al., 2018). The visible spectrum, particularly the blue, red, and RE bands, is associated with plant stress caused by P deficiency (Stein et al., 2014). Leaf water content was detected using indices of NIR, middle-infrared (Hunt & Rock, 1989; Ceccato et al., 2001), and water indices (WIs) such as normalized difference water index (NDWI) (Gao, 1996; McFeeters, 2013; Z. Zhang et al., 2018). As leaf water content decreases, reflectance generally increases across much of NIR spectrum due to the absorption of infrared light by water in the leaves. Consequently, reduced absorption leads to higher reflectance in the NIR region (Carter, 1991). Thus, the spectral slope across the 750–900 nm bands in the NIR is considered an indicator of leaf water content, referred to as the NIR shoulder region index (NSRI) (L.-Y. Liu et al., 2014; D. Xu et al., 2022). Currently, no published studies have explored the use of UAV multispectral imaging that integrates VIs, TFs, and WIs to estimate leaf P concentration in rice.

Previous studies have employed various models, such as random forest, support vector machine, and back propagation artificial neural network, to integrate VIs for estimating leaf P concentration (Y. Zhang et al., 2023). Other approaches include ridge regression and partial least squares regression (J. Zhang et al., 2022) for combining spectral and TFs of UAV images for leaf N concentration monitoring, and artificial neural network for detecting leaf P concentration using band indices (Magalhães et al., 2022). These methods utilize spectral bands and index channels, similar to those in multispectral imagery, to classify and estimate leaf P concentration. However, each spectral band or index shows varying degrees of correlation with leaf P concentration, making them potential indicators for its estimation. To better capture these multivariate relationships, the analytical hierarchy process (AHP)-based multi-criteria evaluation (MCE) model, widely used in ecological and environmental multivariate analyses, has yet to be applied to leaf P concentration estimation.

This study demonstrates three key objectives: (1) to use UAV multispectral imaging data to identify the optimal VIs, TFs, and WIs related to rice leaf P concentration; (2) to evaluate NSRI as one of the WIs contributing to the determination of leaf P concentration in rice, and (3) to demonstrate that combining VIs, TFs, and WIs improves the precision of leaf P concentration estimation using the AHP-based MCE model.

Core Ideas

- Multispectral unmanned aerial vehicle (UAV) imaging was employed to identify the optimal indices related to rice leaf phosphorus concentration.
- The integration of vegetation indices (VIs), texture features (TFs), and water indices (WIs) can improve the accuracy of leaf phosphorus concentration estimation in rice.
- NIR shoulder region index (NSRI), as one of the WIs, contributes to the estimation of phosphorus concentration in rice leaves.

2 | MATERIALS AND METHODS

2.1 | Overall methodology

The leaf P concentration in rice is determined following the procedure outlined in Figure 1. First, UAV multispectral images are processed to generate spectral reflectance orthoimages for blue, green, red, RE, and NIR bands. The VIs and WIs are calculated from various combinations of spectral bands, while TFs are generated from principal component analysis (PCA) using five bands and 16 VIs. In the model construction phase for leaf P concentration estimation, the indices are evaluated against leaf P concentration measurements from field samples to identify those with a high correlation to leaf

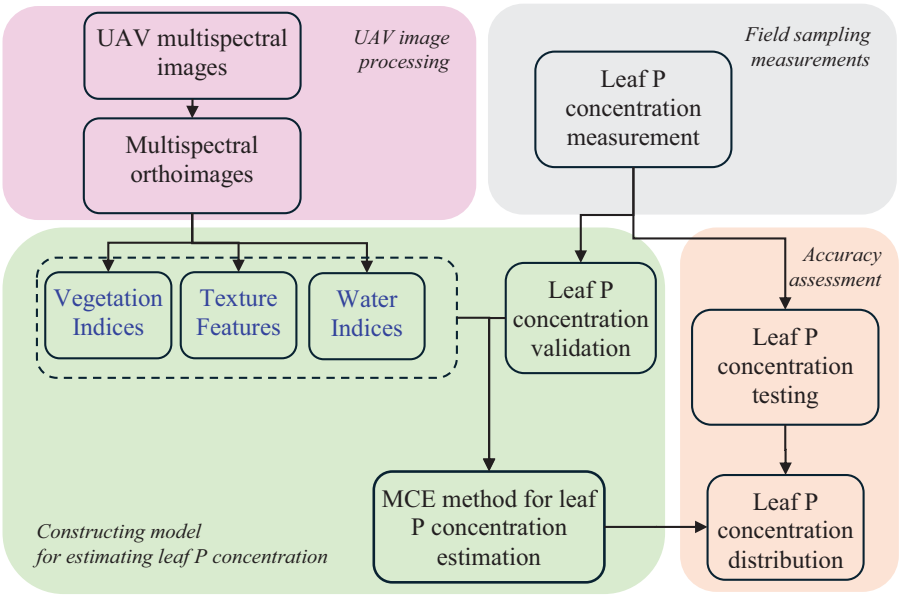

FIGURE 1 Flow chart of estimating rice leaf P concentration in rice from unmanned aerial vehicle (UAV) multispectral images.

P concentration. Subsequently, an integration of appropriate indices into the AHP-based method is used to construct a model for extracting leaf P concentration. The resulting leaf P concentration is assessed for accuracy using the testing leaf P concentration.

2.2 | Study area and experimental design

The experiment was conducted in a rice cultivation area in Phu Tho Province, Vietnam (21°16′35″ N, 105°19′59″ E) (Figure 2). This area is part of the Red River Delta region, characterized by a long-standing tradition of wetland rice cultivation, typical of the northern lowlands of Vietnam. The area has a tropical monsoon climate, where rice is cultivated in two annual cropping seasons: the winter–spring and summer–autumn crop. Additionally, the terrain of the experimental area is flat, which is advantageous for irrigation management. The entire survey site is open and free of obstacles that could interfere with UAV-based aerial imaging. Before measurement and UAV aerial imagery, the field was drained to minimize the impact of water on the spectral reflectance of the rice.

Figure 2 illustrates rice cultivation across 55 plots, each measuring 100 m^2 (10 m × 10 m per plot except for plot T1). Each plot is separated by a 1-m-wide boundary. Two rice varieties, TBR225 and J02, were selected for experimental cultivation, with 27 and 28 plots assigned to each variety, respectively. These high-yielding rice varieties have been and continue to be widely cultivated in Phu Tho, Vietnam. TBR225 is a local traditional rice variety that has been cultivated in this area for a long time, while J02 is a new high-yielding rice variety originating from Japan. Rice plots are fertilized with randomly varying ratios of N, P, and K to manually induce variation in the rice growth rate. These variations in N, P, and K combinations help diversify the values of the sampling points. Additionally, three sample points were randomly selected within each rice plot to collect rice leaves for leaf P concentration extraction. These sample points were distributed across an area of 100m^2 to capture variations in the rice within each plot. The sampling design was intended not only to provide the necessary data for training and testing the model, but also to ensure nondestructively sampled plots.

The experiment was conducted during the milk stage of rice, with field data collection comprising two main tasks: (1) aerial photography using a multispectral UAV and (2) leaf sampling from the rice plots.

2.3 | UAV multispectral image acquisition and processing

The DJI Phantom 4 Multispectral (P4M) drone was used to capture multispectral images of the experimental area. The P4M is a small, vertical takeoff and landing multispectral drone (Figure 3), equipped with six cameras, each with a resolution of 2.08 megapixels (DJI, 2022). One camera captures images in the visible spectrum (red, green, blue), while the other five cameras capture spectral bands, including red, green, blue, RE, and NIR. A sun sensor is integrated on the top of the P4M drone to acquire instantaneous spectral radiation for calibrating multispectral images. The drone is connected to a global navigation satellite system (GNSS) base station to provide a real-time kinetic (RTK) processing for improving

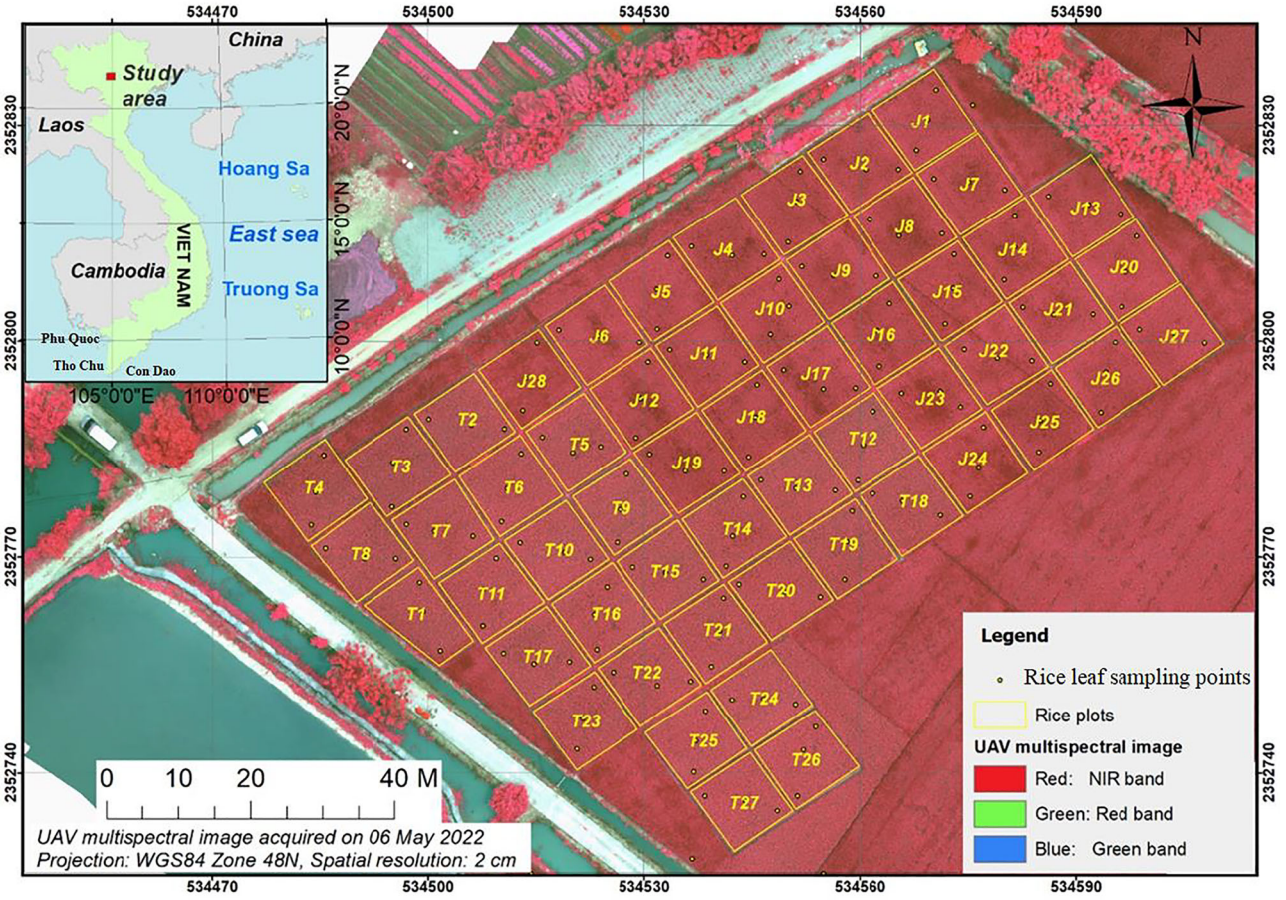

FIGURE 2 Rice plots and leaf sampling points, Phu Tho, Vietnam. NIR, near-infrared; UAV, unmanned aerial vehicle.

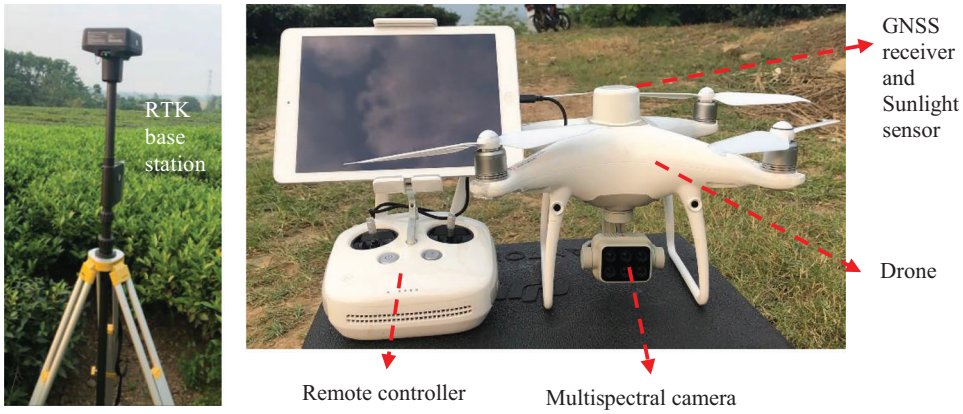

FIGURE 3 Unmanned aerial vehicle (UAV) with a multispectral imaging system. GNSS, global navigation satellite system; RTK, real-time kinematic.

the geometric accuracy of images. The spectral bandwidth and central wavelength of the camera sensor are shown in Table 1.

UAV images were acquired between 10:00 a.m. and 11:45 a.m. on May 6, 2022, under favorable weather conditions, including a sunny day with no cloud cover. The flight altitude during image acquisition was 38 m, with a 75% longitudinal and lateral overlap between images. The aircraft operated in hover-and-capture mode, achieving a ground sampling distance of 2 cm. The multispectral images were radiometrically corrected using data from the sunlight sensor, which is mounted on top of the drone to instantaneously record incident spectral intensity corresponding to the camera's spectral wavelength bands while capturing images. Radiometric correction calculates the surface reflectance of spectral bands

TABLE 1 Parameters of the multispectral sensor for DJI Phantom 4 Multispectral (P4M).

Image bands	Abbreviations	Central wavelength (nm)	Spectral band width (nm)
Blue	B	450 ± 16	20
Green	G	560 ± 16	20
Red	R	650 ± 16	10
Red edge	RE	730 ± 16	10
Near-infrared	NIR	840 ± 26	40

using incident spectral irradiation recorded by the sunlight sensor and reflected spectral irradiation captured by the spectral camera. This correction is applied to each image during image processing. Subsequently, the images were processed using scale-invariant feature transform and structure from motion method to generate a point cloud, digital surface model, and multispectral orthophoto.

2.4 | Leaf sampling and measurement

Simultaneously with the acquisition of multispectral UAV images, three randomly selected sample points were established in each plot to assess leaf P concentration, producing a total of 165 sample points for collecting rice leaves for P concentration extraction. Locations of leaf samples points are accurately measured on the field using a GNSS RTK instrument to synchronize with the multispectral orthoimage obtained from UAV. Leaf P concentration was measured in dried rice leaves using an inductively coupled plasma optical emission spectroscopy (ICP-OES) instrument. Specifically, 10 g of leaves were dried at 200˚C and milled to a particle size smaller than 200 nm. A 0.2 g portion of the resulting powder was mixed with 9 mL of HNO_3 and 1 mL of H_2O_2, heated at 200˚C for 1 h, and diluted to a final volume of 100 mL. The solution was then divided into 10 10 mL aliquots, and standard reference solutions with phosphorus concentrations of 40, 50, 60, 70, and 90 ppm were prepared. Phosphorus concentration (mg/kg) in the fresh leaf samples was determined using ICP-OES by analyzing both the samples and standard solutions. As a result, 70% of P samples (116 samples) are randomly selected for constructing the model to estimate leaf P concentration, while the remaining 30% (49 samples) were used to evaluate the model's accuracy.

2.5 | Index extraction and variable selection

2.5.1 | Vegetation indices

The structural characteristics of the leaves, canopy, and soil background can significantly affect the optical properties of both the leaves and the canopy (Bausch, 1993; Jay et al., 2017). Furthermore, several VIs were selected from the literature to estimate leaf P concentration (Colorado et al., 2020; Mahajan et al., 2016; S. Xu et al., 2023; Zhai et al., 2013; J. Zhang et al., 2022). Consequently, a total of 16 VIs calculated from UAV multispectral images were tested for their correlation with leaf P concentration in rice samples (Table 2). The Pearson correlation coefficient was used to evaluate the relationship between 116 leaf P concentration samples and corresponding values of each VI. Any VIs that were not significantly correlated to leaf P concentration (Pearson's coefficient $r < 0.6$), were excluded from the leaf P concentration estimation model (Trigunasih et al., 2022). Additionally, the 116 VI values were subjected to pairwise comparison to test the similarity of VI pairs using Pearson's correlation coefficient.

2.5.2 | Texture feature

The PCA method was used to process a dataset of 21 images, comprising five UAV spectral bands and 16 VIs to extract images containing the maximum amount of information. The first two principal component images, identified by the highest eigenvalues (PCA1 and PCA2) were processed to generate eight TFs. These TFs were calculated using the gray-level co-occurrence matrix method, employing a 3 × 3 matrix for optimal granularity. A detailed description of eight TFs is provided in Table 3.

2.5.3 | Water indices

In this study, we investigated two WIs to estimate leaf P concentration. The NDWI was calculated using the green (G) and NIR bands (McFeeters, 2013), as shown in Equation (1). The NDWI can be considered an independent index from NDVI, serving as an indicator of vegetation moisture (Gao, 1996). Additionally, the NSRI is defined as the ratio of reflectance at 890 nm to reflectance at 780 nm (H.-H. Liu et al., 2014). The spectral reflectance at wavelengths of 890 and 780 nm corresponds to the NIR and RE band, respectively, in the multispectral UAV images (Equation 2).

$$\mathrm{NDWI} = \frac{R_G - R_{NIR}}{R_G + R_{NIR}} \quad (1)$$

$$\mathrm{NSRI} = \frac{R_{NIR}}{R_{RE}} \quad (2)$$

2.5.4 | Variable selection

In addition to using coefficient of determination (R^2) to evaluate the relationship between variables and leaf P concentration, this study also used the Pearson correlation coefficient

TABLE 2 Vegetation indices used for testing the correlation with leaf P concentration in rice.

No.	Vegetation indices	Formulas	Reference
1	Difference vegetation index	$DVI = R_{NIR} - R_R$	(Jordan, 1969)
2	Enhanced vegetation index	$EVI = 2.5(R_{NIR} - R_R)/(\rho_{NIR} + 6R_R - 7.5R_B + 1)$	(Huete et al., 2002)
3	False color vegetation index	$FCVI = 1.5(2R_{NIR} + R_B - 2R_G)/(2R_G + 2R_B - 2R_{NIR} + 127.5)$	(J. Jiang et al., 2019)
4	Green normalized difference vegetation index	$GNDVI = (R_{NIR} - R_G)/(R_{NIR} + R_G)$	(Buschmann & Nagel, 1993)
5	Leaf chlorophyll index	$LCI = (R_{NIR}/R_{RE}) - 1$	(A. A. Gitelson et al., 2003)
6	Modified chlorophyll absorption in reflectance index	$MCARI = R_{RE} - R_R - 0.2(R_{RE} - \rho_G)R_{RE}/R_R$	(Daughtry et al., 2000)
7	Modified soil adjusted vegetation index	$MSAVI = 0.5(2R_{NIR} + 1 - \sqrt{(2R_{NIR} + 1)^3 - 8(R_{NIR} - R_R)})$	(Qi et al., 1994)
8	Modified simple ratio	$MSR = [(R_{NIR}/R_R) - 1]/[(R_{NIR}/R_R) + 1]$	(Chen, 1996)
9	Normalized difference red edge index	$NDRE = (R_{NIR} - R_{RE})/(R_{NIR} + R_{RE})$	(Gamon & Surfus, 1999)
10	Normalized difference vegetable index	$NDVI = (R_{NIR} - R_R)/(R_{NIR} + R_R)$	(Rouse et al., 1973)
11	Optimized soil adjusted vegetation index	$OSAVI = (R_{NIR} - R_R)/(R_{NIR} + R_R + 0.16)$	(Rondeaux et al., 1996)
12	Photochemical reflectance index	$PRI = (R_G - R_B)/(R_G + R_B)$	(Gamon et al., 1997)
13	Red edge chlorophyll index	$RECI = (R_{NIR} - R_{RE})/R_{RE}$	(A. Gitelson & Merzlyak, 1994)
14	Ratio vegetation index	$RVI = R_{NIR}/R_R$	(Jordan, 1969)
15	Transformed vegetation index	$TVI = (R_G - R_R)/(R_G + R_R)$	(Broge & Leblanc, 2001)
16	Structure-intensive pigment index	$SIPI = (R_{NIR} - R_B)/(R_{NIR} + R_B)$	(Peñuelas et al., 1994)

Note: R_{NIR}, R_{RE}, R_R, R_B, and R_G correspond to spectral reflectance values in the NIR, red edge, red, blue, and green bands, respectively.

TABLE 3 Formulas for calculating texture features from vegetation indices (VIs) and spectral bands.

No.	Texture features	Description	Abbreviations	Formula
1	Contrast	Reflecting the degree of local variation	CON	$\sum_{i=1}^{n}\sum_{j=1}^{n}(i-j)^2 P_{i,j}$
2	Correlation	Capturing the linear relationship between pixel values in the image	COR	$\sum_{i=1}^{n}\sum_{j=1}^{n}\frac{(i-\mathrm{MEA}_j)(j-\mathrm{MEA}_j)P_{i,j}}{\sqrt{\mathrm{VAR}_i}\cdot\sqrt{\mathrm{VAR}_j}}$
3	Dissimilarity	Showing differences in grayscale values	DIS	$\sum_{i=1}^{n}\sum_{j=1}^{n}\lvert i-j\rvert P_{i,j}$
4	Entropy	Expressing the level of randomness in the matrix; second moment	ENT	$-\sum_{i=1}^{n}\sum_{j=1}^{n}P_{i,j}\log P_{i,j}$
5	Homogeneity	Measuring the uniformity within the matrix	HOM	$\sum_{i=1}^{n}\sum_{j=1}^{n}\frac{P_{i,j}}{1+(i-j)^2}$
6	Mean	Representing the average gray level of all pixels in the matrix	MEA	$\sum_{i,j=1}^{n} iP_{i,j}$
7	Second moment	Representing the uniformity of grayscale distribution	SEM	$\sum_{i=1}^{n}\sum_{j=1}^{n}P_{i,j}^2$
8	Variance	Indicating how spread out the values are from the mean	VAR	$\sum_{i=1}^{n}\sum_{j=1}^{n}iP_{i,j}(i-\mathrm{MEA})^2$

Note: i and j represent the row and column of the images, respectively, and $P_{i,j}$ is relative frequency of two adjacent pixels (J. Zhang et al., 2022).

(r). Since a weighted multi-criteria analysis method was used, the selection of individual variables within each group of VIs, WIs, and TFs should consider both positive and negative linear relationships with leaf P concentration. In addition to expert knowledge, the positive–negative relationships also serve as the foundation for determining the weights in the AHP method used in this study. Pearson correlation coefficient measures the strength and direction of the linear relationship between a predictor variable and a target variable, with values ranging from −1 to 1. Predictor variables exhibiting a higher absolute value of r exhibit a stronger linear correlation with the target variable. Consequently, these variables are prioritized over those with lower absolute values of r in the variable selection process based on r (Wang et al., 2021). So, to determine robust VIs, WIs, and TFs for the leaf P concentration of rice, this study selected VIs, WIs, and TFs that showed strong correlations with field leaf P concentration values ($|r| > 0.63$). Additionally, to mitigate the impact of multicollinearity, the correlation matrix is also utilized to select appropriate variables within the VIs. Correlations coefficient above 0.7 typically indicate collinearity concerns (C. Liu et al., 2018).

2.6 | MCE for estimating leaf P concentration

The AHP technique as an MCE approach, effectively integrating geographic information system analysis to estimate leaf P concentration (Y). The AHP is a crucial decision-making technique that helps ensure the coherence of attributes proposed by decision-makers. The process involves conducting pairwise comparisons of factors to establish the hierarchy of their influence (Saaty, 1977), which helps mitigate the effect of multicollinearity. Therefore, AHP does not require testing for multicollinearity (Guo et al., 2024; Hasan et al., 2025; H.-H. Liu et al., 2014). This estimation is performed using a set of multiple criteria X_i, as described in Equation (3). Here, X_i represents criteria drawn from categories of VIs, TFs, and WIs, all of which are closely related to P assimilation

$$Y = \sum_{i=1}^{n} W_i X_i \tag{3}$$

where Y represents leaf P concentration, W_i represents weight of criterion i, X_i represents value of criterion i, and n represents number of criteria.

The pairwise comparison matrix in the AHP model is used to determine the weights of the criteria. The influence of each pair of criteria on leaf P concentration is evaluated based on expert knowledge of the relationship between these factors and leaf P concentration. To assess the role of water, chlorophyll, and texture in relation to the leaf P concentration of rice, this paper employs the MCE model to estimate leaf P concentration under six scenarios, which are combinations of VIs, TFs, and WIs.

2.7 | Accuracy evaluation

The estimated leaf P concentration results were compared with the testing points (30% of the samples) using mean absolute error (MAE) and the least squares method through the root mean square error (RMSE). The MAE and RMSE are defined in Equations (4) and (5), respectively.

$$\mathrm{MAE} = \frac{1}{n}\sum_{i=1}^{n} |v_i| \tag{4}$$

$$\mathrm{RMSE} = \sqrt{\frac{[V_i V_i]}{n}} \tag{5}$$

where V_i represents the actual error at testing point i, calculated as $V_i = \mathrm{LPC_M} - \mathrm{LPC_F}$, n represents the number of sample points used for model evaluation, $\mathrm{LPC_M}$ represents the leaf P concentration estimated by the model, and $\mathrm{LPC_F}$ represents the leaf P concentration obtained from field measurements.

3 | RESULTS

3.1 | Selection of VIs

Table 4 indicates that 14 out of 16 VIs exhibit a strong relationship with leaf P concentration, except for photochemical reflectance index and DVI, which have R^2 values of 0 and 0.36 respectively. Among the 14 VIs, the NDVI is the most strongly correlated with leaf P concentration, with a R^2 value of 0.62. Therefore, NDVI is the most prioritized index for inclusion in the leaf P concentration estimation model. To reduce the number of VI variables included in the model, the correlation matrix (Figure 4) illustrates the similarity between each pair of VIs.

As shown in Figure 4, the VIs demonstrate a very high level of similarity. Among them, modified chlorophyll absorption in reflectance index (MCARI) and NDVI are highly similar with the absolute value of r reaching 0.92 (Figure 4). However, NDVI exhibits the strongest positive correlation with leaf P concentration (Figure 5a), while MCARI is the only index negatively correlated with leaf P concentration (Figure 5b). Therefore, the effects of NDVI and MCARI on leaf P concentration are different. The results show that both NDVI and MCARI were selected for inclusion in the leaf P concentration estimation model

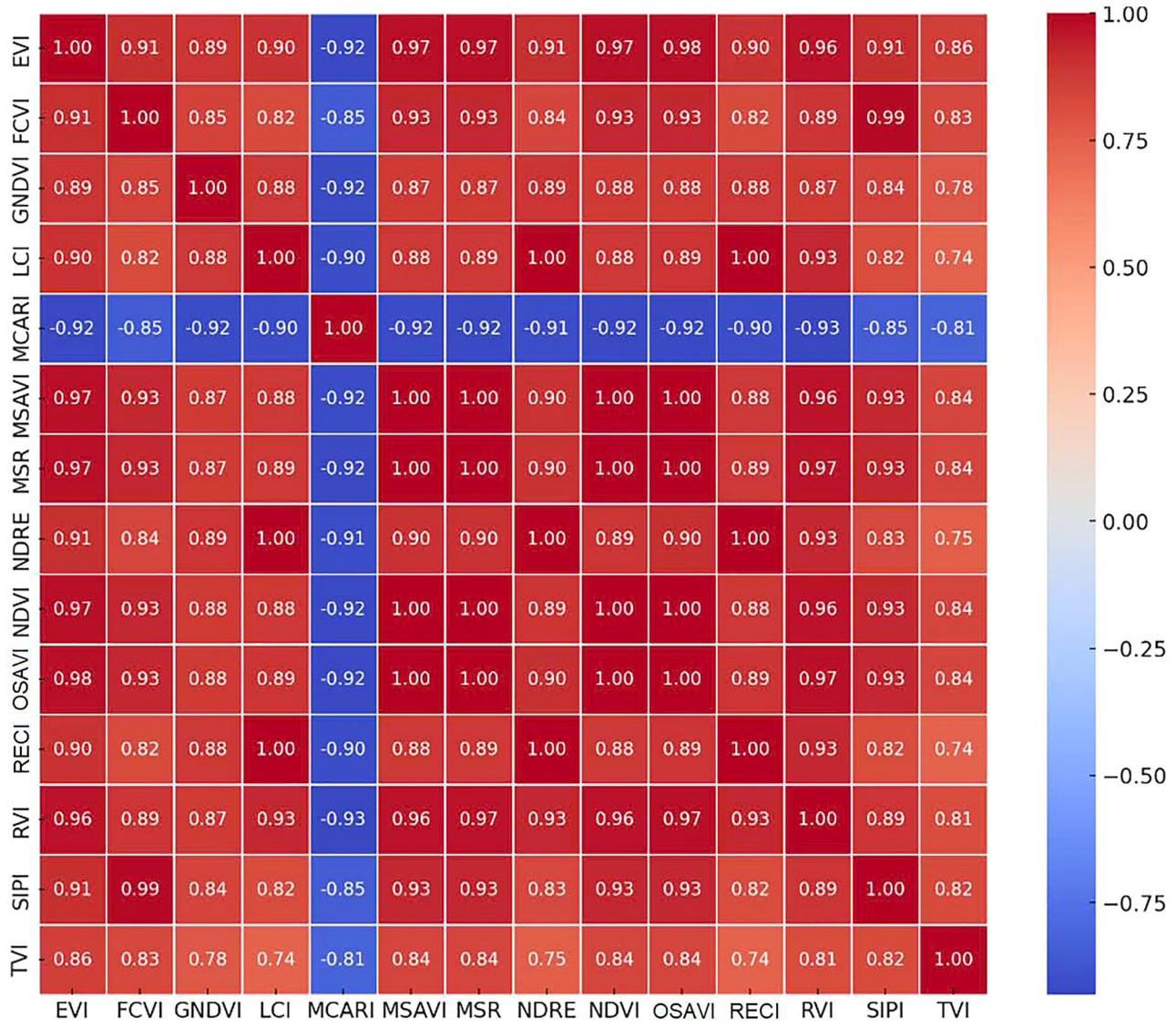

FIGURE 4 Vegetation indices (VIs) correlation matrix. EVI, enhanced vegetation index; FCVI, false color vegetation index; GNDVI, green normalized difference vegetation index; LCI, leaf chlorophyll index; MCARI, modified chlorophyll absorption in reflectance index; MSAVI, modified soil adjusted vegetation index; MSR, modified simple ratio; NDRE, normalized difference red edge; NDVI, normalized difference vegetation index; OSAVI, optimized soil adjusted vegetation index; RECI, red-edge chlorophyll index; RVI, ratio vegetation index; SIPI, structure-intensive pigment index; TVI, transformed vegetation index.

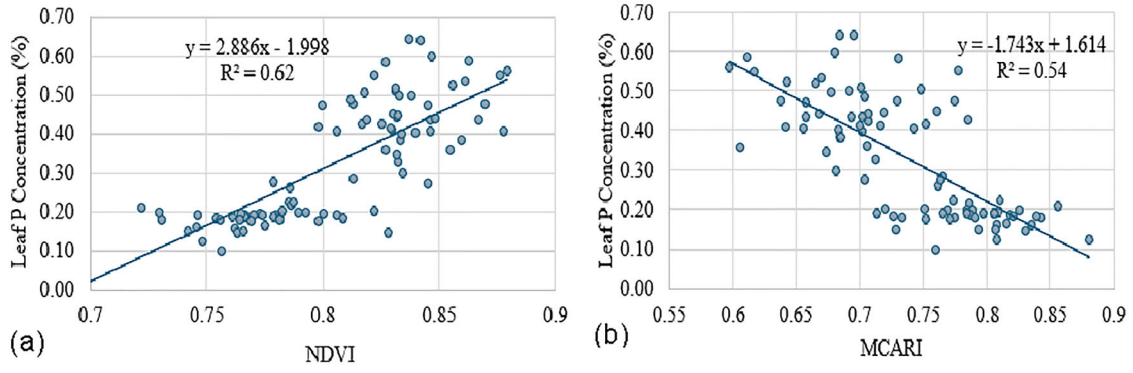

FIGURE 5 Relationship between (a) leaf P concentration and normalized difference vegetation index (NDVI) and (b) leaf P concentration and modified chlorophyll absorption in reflectance index (MCARI).

TABLE 4 Relationship between vegetation indices (VIs) and leaf P concentration.

Number	VIs	R^2	r	Number	VIs	R^2	r
1	DVI	0.36	0.60	9	NDVI	0.62	0.78
2	EVI	0.52	0.72	10	OSAVI	0.61	0.78
3	FCVI	0.50	0.71	11	PRI	0.00	−0.06
4	GNDVI	0.47	0.68	12	RECI	0.54	0.73
5	MCARI	0.54	−0.73	13	RVI	0.60	0.77
6	MSAVI	0.61	0.78	14	TVI	0.40	0.63
7	MSR	0.61	0.78	15	SIPI	0.52	0.72
8	NDRE	0.55	0.74	16	LCI	0.54	0.73

Abbreviations: DVI, difference vegetation index; EVI, enhanced vegetation index; FCVI, false color vegetation index; GNDVI, green normalized difference vegetation index; LCI, leaf chlorophyll index; MCARI, modified chlorophyll absorption in reflectance index; MSAVI, modified soil adjusted vegetation index; MSR, modified simple ratio; NDRE, normalized difference red edge; NDVI, normalized difference vegetation index; OSAVI, optimized soil adjusted vegetation index; PRI, photochemical reflectance index; RECI, red-edge chlorophyll index; RVI, ratio vegetation index; SIPI, structure-intensive pigment index; TVI, transformed vegetation index.

TABLE 5 Texture features (TFs) and leaf P concentration relationship.

Number	TFs	R^2	r	Number	TFs	R^2	r
1	CON	0.13	−0.36	5	HOM	0.12	0.35
2	COR	0.08	0.28	6	MEA	0.64	0.80
3	DIS	0.13	−0.36	7	SEM	0.16	0.40
4	ENT	0.30	−0.55	8	VAR	0.16	−0.40

Abbreviations: CON, contrast; COR, correlation; DIS, dissimilarity; ENT, entropy; HOM, homogeneity; MEA, mean; SEM, second moment; VAR, variance.

3.2 | Selection of TFs

PCA1 and PCA2 are the two principal components derived from 16 VIs and five bands of UAV multispectral data. PCA1 and PCA2 exhibit correlations with leaf P concentration of 0.74 and 0.73, respectively. Therefore, PCA1 was selected for calculating the TFs. The relationship between TFs and leaf P concentration is presented in Table 5. Table 5 indicates that the relationship between TFs and leaf P concentration is generally low to moderate, except for the mean (MEA) index, which has a R^2 value of 0.64. Therefore, MEA was selected as the representative TF demonstrating a strong relationship with leaf P concentration (Figure 6).

3.3 | Selection of WIs

Figure 7 indicates that the relationship between NDWI, NSRI, and leaf P concentration is strong, with R^2 values of 0.55 and 0.64, respectively. However, while NDWI exhibits a negative correlation with leaf P concentration, NSRI shows a positive correlation with leaf P concentration. Therefore, both NDWI and NSRI are considered criteria for the leaf P concentration estimation model.

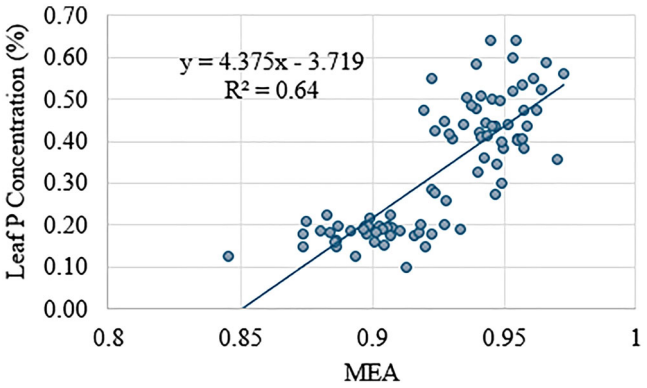

FIGURE 6 Relationship between mean (MEA) and leaf P concentration.

3.4 | Model for leaf P concentration estimation in rice

The AHP-based MCE technique is chosen as the model for estimating leaf P concentration (Equation 3). The criteria include NDVI and MCARI, representing the VIs group; MEA, representing the TFs group; and NDWI and NSRI, representing the WIs group. Figure 8 illustrates the R^2 and r value for each criterion in relation to leaf P concentration.

Figure 8 demonstrates a strong relationship between the five criteria and leaf P concentration. However, while NDVI, MEA, and NSRI exhibit positive correlations, MCARI and NDWI show negative correlations. Overall, the group with positive correlations has higher values compared to the group with negative correlations. To evaluate the contribution of index groups to the estimated leaf P concentration using the AHP-based MCE model, four scenarios (S1, S2, S3, and S4) are constructed from five criteria, as shown in Table 6. The weights *Wi* were determined using the AHP model. The results of the weights, RMSE, MAE, and R^2 values of the models are presented in Table 7.

Abbreviations: MAE, mean absolute error; MCARI, modified chlorophyll absorption in reflectance index; MCE, multi-criteria evaluation; MEA, mean; NDVI, normalized difference vegetation index; NDWI, normalized difference water index; NSRI, NIR shoulder region index; RMSE, root mean square error.

Table 7 provides information on the MCE scenarios for estimating P content, based on factors such as NDVI, MCARI, MEA, NSRI, and NDWI. It shows that MEA plays the most important role in all scenarios with the highest weight ranging from 0.41 in S4 to 0.59 in S1. Moreover, Table 7 also shows

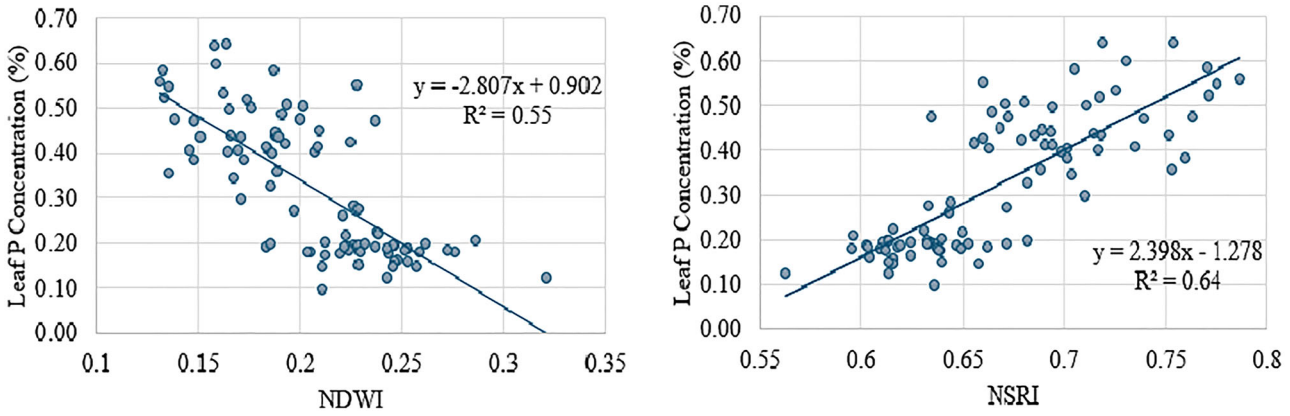

FIGURE 7 Relationship between (a) leaf P concentration and normalized difference water index (NDWI) and (b) leaf P concentration and NIR shoulder region index (NSRI).

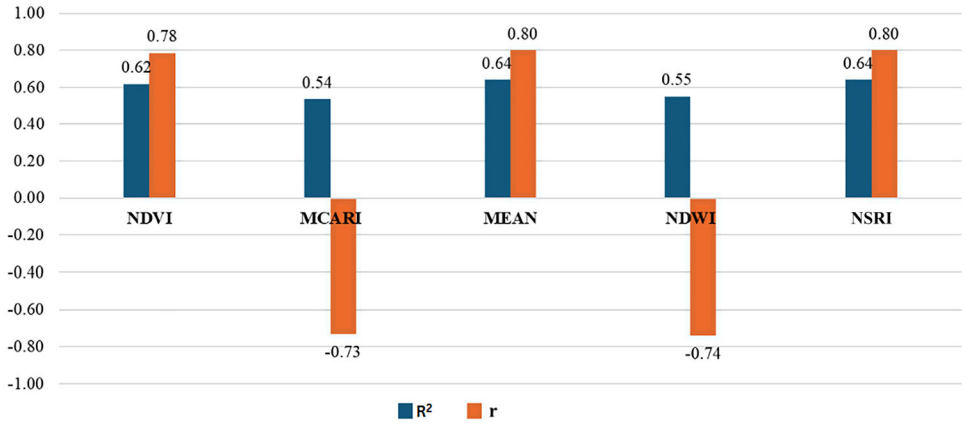

FIGURE 8 The relationship between the indices (criteria) and leaf P concentration. MCARI, modified chlorophyll absorption in reflectance index; NDVI, normalized difference vegetation index; NDWI, normalized difference water index, NSRI, NIR shoulder region index.

TABLE 6 Scenarios of multi-criteria evaluation (MCE)

Scenarios of the MCE model	Characteristics	Equation
S1	The indices in each of VIs and TFs	W1.NDVI + W2. MCARI + W3.MEA
S2	VIs, TFs, and WIs, which have negative correlation with leaf P concentration	W1.NDVI + W2. MCARI + W3.MEA + W5.NDWI
S3	VIs, TFs, and WIs, which have positive correlation with leaf P concentration	W1. NDVI + W2.MCARI + W3. MEA + W4. NSRI
S4	All of VIs, TFs, and WIs	W1. NDVI + W2. MCARI + W3.MEA + W4.NSRI + W5.NDWI

Note: W1 represents weight of NDVI, W2 represents weight of MEA, W3 represents weight of NSRI, W4 represents weight of NDWI, and W5 represents weight of MCARI.

Abbreviations: MCARI, modified chlorophyll absorption in reflectance index; MEA, mean; NDVI, normalized difference vegetation index; NDWI, normalized difference water index; NSRI, NIR shoulder region index; TFs, texture features indices; VIs, vegetation indices; WIs, water indices.

that the relationship between MEA and leaf P concentration is the strongest. When considering indices within the same group, the NDVI in the VIs group has a higher weight than the MCARI. Similarly, in the WIs group, the NSRI holds a higher weight compared to NDWI in S4.

Moreover, the R^2 value increases from 0.70 in S1 to 0.75 in S4, reflecting a significant improvement in the model's ability to explain the relationship between the factors and leaf P content. Additionally, the RMSE and MAE decrease slightly from 0.041 of RMSE and 0.038 of MAE in S1 to 0.035 of RMSE

TABLE 7 The weights W_i using analytic hierarchy process (AHP) model.

	Weight							
MCE	**NDVI**	**MCARI**	**MEA**	**NSRI**	**NDWI**	R^2	**RMSE (%)**	**MAE**
S1	0.25	0.16	0.59	–	–	0.70	0.041	0.038
S2	0.23	0.10	0.48	–	0.19	0.72	0.043	0.036
S3	0.19	0.11	0.48	0.22	–	0.72	0.039	0.033
S4	0.18	0.08	0.41	0.17	0.15	0.75	0.035	0.030

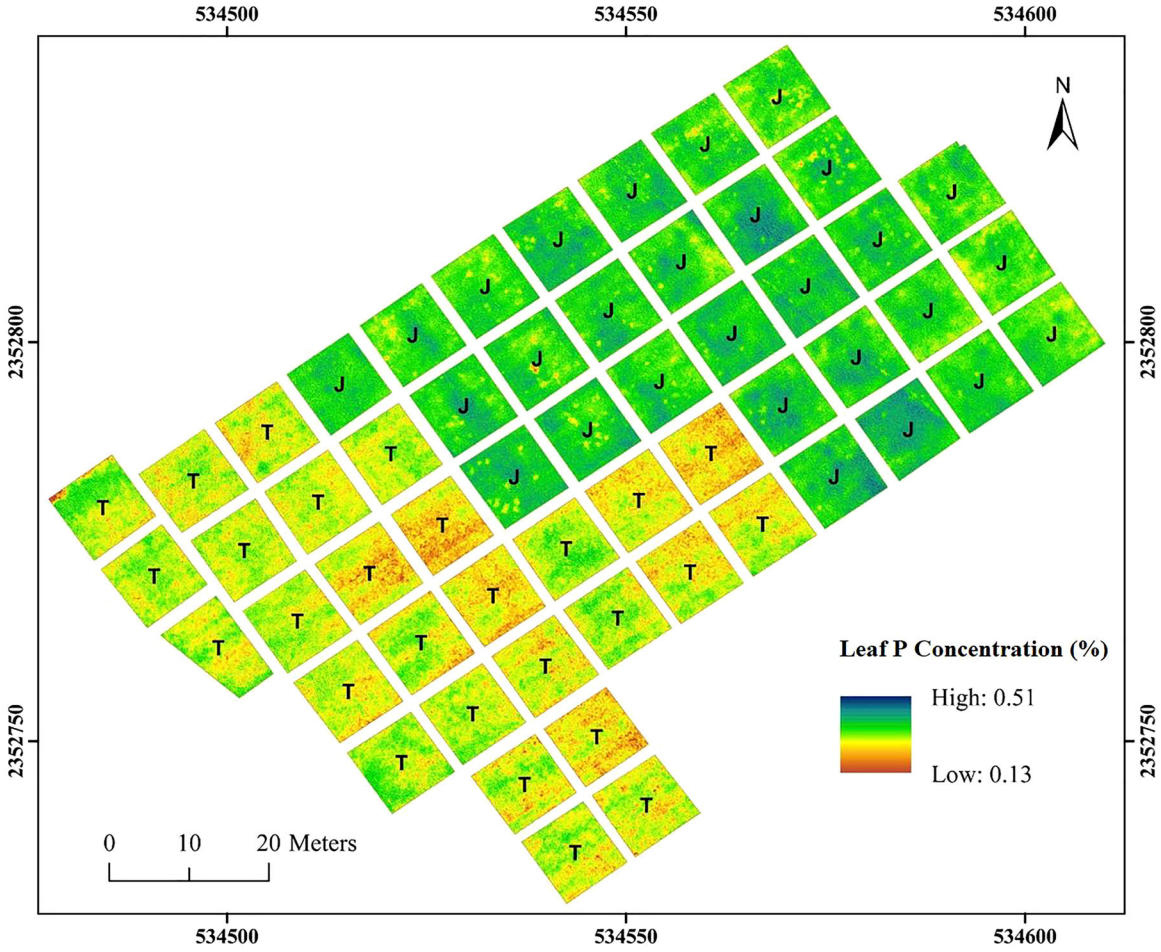

FIGURE 9 Leaf P concentration, which was extracted by combining vegetation indices (VIs), texture features indices (TFs), and water indices (WIs) (T, TBR225; J, J02).

and 0.003 of MAE in S4, suggesting that the model's error reduces as additional factors are included. These results indicate that the model becomes more accurate across scenarios. Figure 9 corresponding to S4 represents the best scenarios.

Figure 10 indicates that the leaf P concentration of rice variety J02 ranges from 0.343% to 0.462%, while that of rice variety TBR225 ranges from 0.272% to 0.442%. Overall, the leaf P concentration of variety J02 is higher than that of variety TBR225.

4 | DISCUSSION

4.1 | Comparison of variable importance

In this study, we examined the relationship between 26 spectral variables and leaf P concentration, including 16 VIs, eight TFs, and two WIs. Among these, five indices were selected as criteria in the leaf P concentration estimation models, namely NDVI, MEA, NSRI, NDWI, and MCARI.

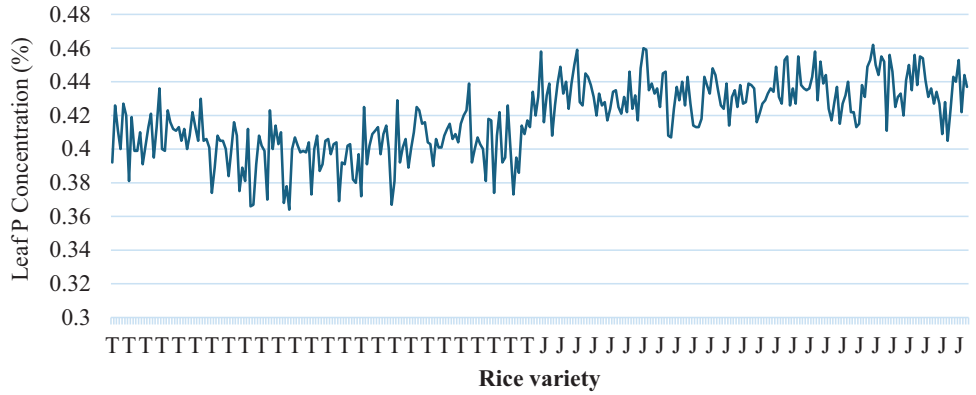

FIGURE 10 The leaf P concentration of rice varieties (T, TBR225; J, Japonica 02 [J02]).

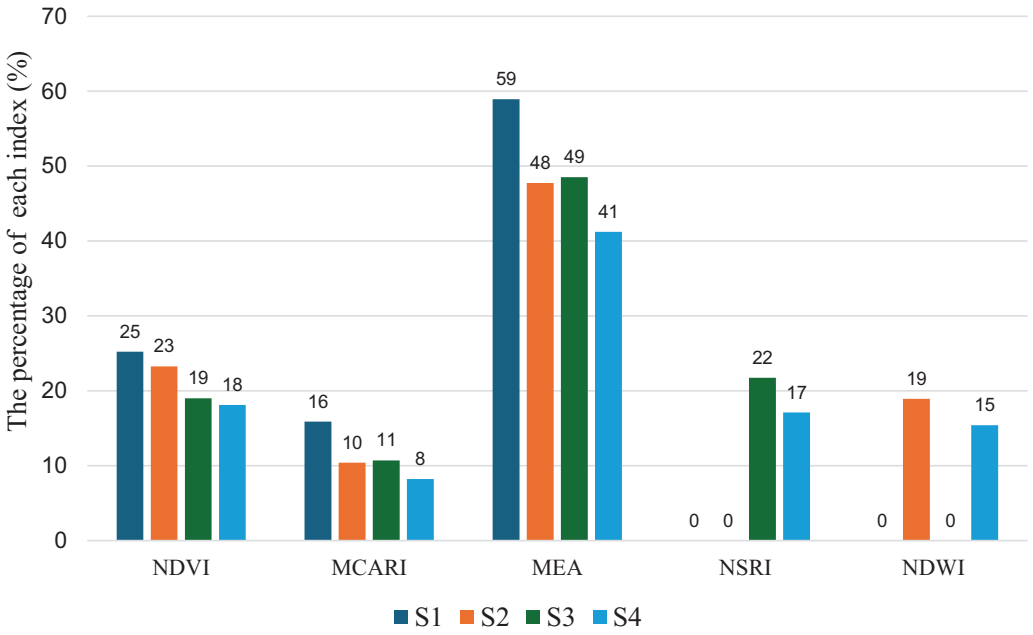

FIGURE 11 The percentage contribution of criteria to the leaf P concentration estimation model. MCARI, modified chlorophyll absorption in reflectance index; MEA, mean; NDVI, normalized difference vegetation index; NDWI, normalized difference water index; NSRI, NIR shoulder region index.

Several studies have demonstrated that combining VIs and TFs significantly enhances the accuracy of rice yield estimation models (Zhou et al., 2022) and N content estimation in crops (J. Zhang et al., 2022). By integrating spectral and textural information, these models can capture both biochemical and structural traits of the plants, leading to more reliable N, K, and P assessments. In the scenarios presented in Table 7, these results indicate that the integration of VIs and TFs has enhanced the accuracy and quality of the model in estimating leaf P concentration.

Figure 11 shows that the NDWI has distributed at 19% in S2 and 15% in S4. Therefore, NDWI can be considered an important independent index to NDVI (Gao, 1996), as evidenced by the results in S2. When NDWI was combined with indices from NDVI, MCARI, and MEA, the results of the MCE model were significantly improved (Table 7).

In addition, the NSRI has been used as an indicator of variations in leaf water content. The NSRI index has lower sensitivity compared to SWIR and NDWI. However, its effectiveness also depends on the study subject and the degree of leaf water variation (L.-Y. Liu et al., 2014). The NSRI appears only in S3 and S4 with contribution of 22% and 17%, respectively (Figure 11), reflecting the plant's stress level, particularly under conditions of water or nutrient deficiency (Huang et al., 2015).

On the other hand, a comparison of correlation and the contribution of the two WIs to MCE reveals distinct differences. The relationship between NSRI and leaf P concentration

($R^2 = 0.64$) is stronger than that between NDWI and leaf P concentration ($R^2 = 0.55$). In S4 of Figure 11, NSRI contributed 17% to leaf P concentration estimation, while NDWI contributed only 15%. These findings indicate that within the WIs group, NSRI demonstrates greater sensitivity than NDWI for estimating leaf P concentration. This outcome demonstrates the novel contribution of this study in identifying a water-related index that performs well in determining leaf P concentration in rice.

4.2 | Evaluation of modeling variables and accuracy

Table 7 suggests that as the model's ability to explain the data improves (higher R^2), its prediction accuracy also increases (lower RMSE). This trend highlights that the model is optimized with each scenario, especially in S4, where the combination of factors like NDWI and NSRI leads to the best results, offering both the highest R^2 (0.75) and the lowest RMSE (0.035). NDWI captures the water content in vegetation and helps differentiate water bodies from land areas, which can be crucial in agricultural and environmental studies, especially in assessing P concentrations that often correlate with water systems. NDWI is widely used in environmental studies for assessing vegetation health and water stress (Gao, 1996). Research has shown that NDWI play a significant role in enhancing model accuracy for predicting various leaf P concentration. Research indicates that plants experiencing water stress often exhibit reduced nutrient absorption capabilities, including P (Aguswan et al., 2022). By accurately measuring water content through NDWI, models can better predict the P in plant tissues, as water stress can limit the mobility of nutrients within the soil and their uptake by roots (Onprasonk et al., 2023). Similarly, NSRI has been recognized as a useful index for determining plant stress and nutrient uptake, including P. Studies have indicated that NSRI can help monitor the physiological responses of these plants to varying P levels (Crusciol et al., 2021). Its inclusion in models typically improves predictions of ecological factors, particularly when modeling stress-sensitive variables like P in soil and water.

In summary, NDWI and NSRI can be integrated into models for assessing and predicting rice P. Additionally, incorporating VIs, TFs, and WIs, the model becomes better suited to predict leaf P concentration in rice with higher precision, which explains the trend observed in the data for S4.

4.3 | Analysis Leaf P Concentration

TBR225, a popular rice variety in Northern Vietnam, is known for its susceptibility to certain diseases but also exhibits specific traits that may influence nutrient uptake, including P (Duy et al., 2021). The leaf P concentration of rice varieties J02 and TBR225 reveals notable differences in nutrient uptake, with variety J02 demonstrating higher P levels than variety TBR225. This difference may be attributed to the inherent characteristics of the varieties, with Japonica rice (variety J02) showing better adaptability to environmental conditions and potentially greater nutrient uptake efficiency compared to Indica rice varieties such as TBR225 (Das et al., 2020). These findings suggest that rice variety J02 may be more efficient in utilizing P, which could play a crucial role in optimizing nutrient management in rice cultivation.

4.4 | Research limitations and future prospects

The UAV multispectral technology offers an innovative remote sensing approach essential for advancing precision agriculture research. This study was conducted on a pilot scale within a small area (5500 m^2) with a limited experimental dataset comprising 165 sampling points. Moreover, UAVs are expensive, and data collection is time-consuming and labor-intensive. Therefore, expanding the sampling to include a larger number of points and integrating satellite remote sensing technology, such as Worldview-3, could enhance model accuracy on a large scale, and facilitate continuous monitoring of leaf P concentration in rice at different growth stages.

In this paper, indices from the VIs, TFs, and WIs groups were combined in various scenarios to improve the estimation accuracy of leaf P concentration for two different rice varieties. The leaf P concentration of the rice varieties, derived from UAV multispectral imagery, serves as a basis for assessing nutrient deficiencies or excesses in rice plants. This information enables precise fertilizer application decisions, tailored to each rice variety and, in future studies, to individual paddy fields.

5 | CONCLUSION

Based on the outcomes from this study, it can be concluded that monitoring leaf P concentration in rice plants using UAV data is feasible. However, the accuracy of this approach depends on the effective combination of VIs, TFs, and WIs.

WIs play a significant role in leaf P concentration estimation, as multispectral UAV imagery not only captures variations in VIs and TF, but also enables WIs, derived from specific spectral bands, to further delineate leaf texture characteristics. This enhances the ability of remote sensing data to detect P signals. Therefore, fusion indicators, derived from five parameters, were selected based on their strong relationship with rice leaf P concentration using the AHP-based MCE method, including two VIs (NDVI and MCARI), one TF (MEA) and two WIs (NDWI and NSRI). This integration can improve the accuracy of leaf P concentration estimation.

Understanding the nutrient uptake differences between rice varieties TBR225 and J02 is crucial for improving agricultural productivity and sustainability, informing decisions on rice variety selection and fertilization strategies in various agroecological zones.

AUTHOR CONTRIBUTIONS

Canh Van Le: Conceptualization; data curation; formal analysis; methodology; writing—original draft. **Lan Thi Pham**: Conceptualization; data curation; formal analysis; methodology; supervision; validation; writing—original draft; writing—review and editing.

ACKNOWLEDGMENTS

This research was supported by Hanoi University of Mining and Geology through the institution-level project, Grant Number T24-30.

CONFLICT OF INTEREST STATEMENT

The authors declare no conflicts of interest.

ORCID

Canh Van Le https://orcid.org/0000-0002-8113-9949
Lan Thi Pham https://orcid.org/0000-0003-3982-1896

REFERENCES

Aguswan, Y., Gumiri, S., Sukarna, R. M., & Permana, I. (2022). Mapping beje pond as fish source in a tropical peat swamp using Landsat 8 OLI-TIRS imagery. *IOP Conference Series: Earth and Environmental Science*, *1119*(1), 012082. https://doi.org/10.1088/1755-1315/1119/1/012082

Ban, S., Liu, W., Tian, M., Wang, Q., Yuan, T., Chang, Q., & Li, L. (2022). Rice leaf chlorophyll content estimation using UAV-based spectral images in different regions. *Agronomy*, *12*(11), 2832. https://doi.org/10.3390/agronomy12112832

Barbosa, E. R., Tomlinson, K. W., Carvalheiro, L. G., Kirkman, K., de Bie, S., Prins, H. H., & van Langevelde, F. (2014). Short-term effect of nutrient availability and rainfall distribution on biomass production and leaf nutrient content of savanna tree species. *PLoS One*, *9*(3), e92619. https://doi.org/10.1371/journal.pone.0092619

Bausch, W. C. (1993). Soil background effects on reflectance-based crop coefficients for corn. *Remote Sensing of Environment*, *46*, 213–222. https://doi.org/10.1016/0034-4257(93)90096-G

Broge, N. H., & Leblanc, E. (2001). Comparing prediction power and stability of broadband and hyperspectral vegetation indices for estimation of green leaf area index and canopy chlorophyll density. *Remote Sensing of Environment*, *76*(2), 156–172. https://doi.org/10.1016/S0034-4257(00)00197-8

Buschmann, C., & Nagel, E. (1993). In vivo spectroscopy and internal optics of leaves as basis for remote sensing of vegetation. *International Journal of Remote Sensing*, *14*(4), 711–722. https://doi.org/10.1080/01431169308904370

Carter, G. A. (1991). Primary and secondary effects of water content on the spectral reflectance of leaves. *American Journal of Botany*, *78*(7), 916–924. https://doi.org/10.1002/j.1537-2197.1991.tb14495.x

Ceccato, P., Flasse, S., Tarantola, S., Jacquemoud, S., & Grégoire, J.-M. (2001). Detecting vegetation leaf water content using reflectance in the optical domain. *Remote Sensing of Environment*, *77*, 22–33. https://doi.org/10.1016/S0034-4257(01)00191-2

Chen, J. M. (1996). Evaluation of vegetation indices and a modified simple ratio for boreal applications. *Canadian Journal of Remote Sensing*, *22*(3), 229–242. https://doi.org/10.1080/07038992.1996.10855178

Colorado, J. D., Cera-Bornacelli, N., Caldas, J. S., Petro, E., Rebolledo, M. C., Cuellar, D., Calderon, F., Mondragon, I. F., & Jaramillo-Botero, A. (2020). Estimation of nitrogen in rice crops from UAV-captured images. *Remote Sensing*, *12*(20), 3396. https://doi.org/10.3390/rs12203396

Crusciol, C. A. C., Portugal, J. R., Bossolani, J. W., Moretti, L. G., Fernandes, A. M., Garcia, J. L. N., Garcia, G. L. D. B., Pilon, C., & Cantarella, H. (2021). Dynamics of macronutrient uptake and removal by modern peanut cultivars. *Plants*, *10*(10), 2167. https://doi.org/10.3390/plants10102167

Das, S., Gwon, H. S., Khan, M. I., Jeong, S. T., & Kim, P. J. (2020). Steel slag amendment impacts on soil microbial communities and activities of rice (*Oryza sativa* L.). *Scientific Reports*, *10*(1), 6746. https://doi.org/10.1038/s41598-020-63783-1

Daughtry, C. S. T., Walthall, C. L., Kim, M. S., de Colstoun, E. B., & McMurtrey, J. E. (2000). Estimating corn leaf chlorophyll concentration from leaf and canopy reflectance. *Remote Sensing of Environment*, *74*(2), 229–239. https://doi.org/10.1016/S0034-4257(00)00113-9

Delavarpour, N., Koparan, C., Nowatzki, J., Bajwa, S., & Sun, X. (2021). A technical study on UAV characteristics for precision agriculture applications and associated practical challenges. *Remote Sensing*, *13*(6), 1204. https://doi.org/10.3390/rs13061204

DJI. (2022). *P4 multispectral plant intelligence for targeted action*. DJI.

Dumitru, F. (2023). Current status and prospects of research on UAV remote sensing inversion of rice agronomic physical and chemical parameters. *Academic Journal of Earth Sciences*, *1*(2), 19–27. https://doi.org/10.61784/ajes231208

Duy, P. N., Lan, D. T., Pham Thu, H., Thi Thu, H. P., Nguyen Thanh, H., Pham, N. P., Auguy, F., Bui Thi Thu, H., Manh, T. B., Cunnac, S., & Pham, X. H. (2021). Improved bacterial leaf blight disease resistance in the major elite Vietnamese rice cultivar TBR225 via editing of the OsSWEET14 promoter. *PLoS One*, *16*(9), e0255470. https://doi.org/10.1371/journal.pone.0255470

Faustin, N. K. (2024). Applications of remote sensing in precision agriculture. *Journal of Engineering and Scientific Research*, *3*(1), 29–33.

Gamon, J. A., Serrano, L., & Surfus, J. S. (1997). The photochemical reflectance index: An optical indicator of photosynthetic radiation use efficiency across species, functional types, and nutrient levels. *Oecologia*, *112*(4), 492–501. https://doi.org/10.1007/s004420050337

Gamon, J. A., & Surfus, J. S. (1999). Assessing leaf pigment content and activity with a reflectometer. *New Phytologist*, *143*(1), 105–117. https://doi.org/10.1046/j.1469-8137.1999.00424.x

Gao, B.-C. (1996). NDWI—A normalized difference water index for remote sensing of vegetation liquid water from space. *Remote Sensing of Environment*, *58*(3), 257–266. https://doi.org/10.1016/s0034-4257(96)00067-3

Gitelson, A., & Merzlyak, M. N. (1994). Quantitative estimation of chlorophyll-a using reflectance spectra: Experiments with autumn chestnut and maple leaves. *Journal of Photochemistry and Photobiology B: Biology*, *22*(3), 247–252. https://doi.org/10.1016/1011-1344(93)06963-4

Gitelson, A. A., Gritz, Y., & Merzlyak, M. N. (2003). Relationships between leaf chlorophyll content and spectral reflectance and

algorithms for non-destructive chlorophyll assessment in higher plant leaves. *Journal of Plant Physiology*, *160*(3), 271–282. https://doi.org/10.1078/0176-1617-00887

Guo, L., Xiong, S., Mills, B. J. W., Isson, T., Yang, S., Cui, J., Wang, Y., Jiang, L., Xu, Z., Cai, C., Deng, Y., Wei, G., & Zhao, M. (2024). Acceleration of phosphorus weathering under warm climates. *Science Advances*, *10*, 1–8. https://doi.org/10.1126/sciadv.adm7773

Hasan, M. M., Talha, M., Akter, M. M., Ferdous, M. T., Mojumder, P., Roy, S. K., & Refat Nasher, N. M. (2025). Assessing the performance of machine learning and analytical hierarchy process (AHP) models for rainwater harvesting potential zone identification in hilly region, Bangladesh. *Journal of Asian Earth Sciences: X*, *13*, 100189. https://doi.org/10.1016/j.jaesx.2024.100189

Hoque, M. M., Ajwa, H., Othman, M., Smith, R., & Cahn, A. M. (2010). Yield and postharvest quality of lettuce in response to nitrogen, phosphorus, and potassium fertilizers. *Hortscience*, *45*(10), 1539–1544. https://doi.org/10.21273/HORTSCI.45.10.1539

Huang, L.-S., Ju, S.-C., Zhao, J.-L., Zhang, D.-Y., Hong, Q., Teng, L., Yang, F., & Zuo, Y. (2015). Hyperspectral measurements for estimating vertical infection of yellow rust on winter wheat plant. *International Journal of Agriculture and Biology*, *17*(06), 1237–1242. https://doi.org/10.17957/ijab/15.0034

Huete, A., Didan, K., Miura, T., Rodriguez, E. P., Gao, X., & Ferreira, L. G. (2002). Overview of the radiometric and biophysical performance of the MODIS vegetation indices. *Remote Sensing of Environment*, *83*(1), 195–213. https://doi.org/10.1016/S0034-4257(02)00096-2

Hunt, E., Jr., & Rock, B. (1989). Detection of changes in leaf water content using near- and middle-infrared reflectances. *Remote Sensing of Environment*, *30*(1), 43–54. https://doi.org/10.1016/0034-4257(89)90046-1

Irfan, M., Aziz, T., Maqsood, M. A., Bilal, H. M., Siddique, K. H. M., & Xu, M. (2020). Phosphorus (P) use efficiency in rice is linked to tissue-specific biomass and P allocation patterns. *Scientific Reports*, *10*(1), 4278. https://doi.org/10.1038/s41598-020-61147-3

Jay, S., Gorretta, N., Morel, J., Maupas, F., Bendoula, R., Rabatel, G., Dutartre, D., Comar, A., & Baret, F. (2017). Estimating leaf chlorophyll content in sugar beet canopies using millimeter- to centimeter-scale reflectance imagery. *Remote Sensing of Environment*, *198*, 173–186. https://doi.org/10.1016/j.rse.2017.06.008

Jiang, J., Cai, W., Zheng, H., Cheng, T., Tian, Y., Zhu, Y., Ehsani, R., Hu, Y., Niu, Q., Gui, L., & Yao, X. (2019). Using digital cameras on an unmanned aerial vehicle to derive optimum color vegetation indices for leaf nitrogen concentration monitoring in winter wheat. *Remote Sensing*, *11*(22), 2667. https://doi.org/10.3390/rs11222667

Jiang, S., Tang, Y., Fan, R., Bai, S., Wang, X., Huang, Y., Li, W., & Ji, W. (2023). Response of *Carex breviculmis* to phosphorus deficiency and drought stress. *Frontiers in Plant Science*, *14*, 1203924. https://doi.org/10.3389/fpls.2023.1203924

Jordan, C. F. (1969). Derivation of leaf-area index from quality of light on the forest floor. *Ecology*, *50*(4), 663–666. https://doi.org/10.2307/1936256

Khose, S. B., & Mailapalli, D. R. (2024). UAV-based multispectral image analytics and machine learning for predicting crop nitrogen in rice. *Geocarto International*, *39*(1),. https://doi.org/10.1080/10106049.2024.2373867

Li, D., Wang, C., Jiang, H., Peng, Z., Yang, J., Su, Y., Song, J., & Chen, S. (2018). Monitoring litchi canopy foliar phosphorus content using hyperspectral data. *Computers and Electronics in Agriculture*, *154*, 176–186. https://doi.org/10.1016/j.compag.2018.09.007

Liaghat, S., & Balasundram, S. K. (2010). A review: The role of remote sensing in precision agriculture. *American Journal of Agricultural and Biological Sciences*, *5*(1), 50–55. https://doi.org/10.3844/ajabssp.2010.50.55

Liu, C., Zhang, Z., & Balay, J. W. (2018). Posterior assessment of reference gages for water resources management using instantaneous flow measurements. *Science of the Total Environment*, *634*, 12–19. https://doi.org/10.1016/j.scitotenv.2018.03.312

Liu, H.-H., Yeh, Y.-Y., & Huang, J.-J. (2014). Correlated analytic hierarchy process. *Mathematical Problems in Engineering*, *2014*(1), 1–7. https://doi.org/10.1155/2014/961714

Liu, L.-Y., Huang, W.-J., Pu, R.-L., & Wang, J.-H (2014). Detection of internal leaf structure deterioration using a new spectral ratio index in the near-infrared shoulder region. *Journal of Integrative Agriculture*, *13*(4), 760–769. https://doi.org/10.1016/S2095-3119(13)60385-8

Liu, Y., Hatou, K., Aihara, T., Kurose, S., Akiyama, T., Kohno, Y., Lu, S., & Omasa, K. (2021). A robust vegetation index based on different UAV RGB images to estimate SPAD values of naked barley leaves. *Remote Sensing*, *13*(4), 686. https://doi.org/10.3390/rs13040686

Lu, J., Yang, T., Su, X., Qi, H., Yao, X., Cheng, T., Zhu, Y., Cao, W., & Tian, Y. (2020). Monitoring leaf potassium content using hyperspectral vegetation indices in rice leaves. *Precision Agriculture*, *21*(2), 324–348. https://doi.org/10.1007/s11119-019-09670-w

Magalhães, L. P. D., Trevisan, L. R., Gomes, T. M., & Rossi, F. (2022). Use of digital images to classify leaf phosphorus content in grape tomatoes. *Engenharia Agrícola*, *42*(spe). https://doi.org/10.1590/1809-4430-eng.agric.v42nepe20210147/2022

Mahajan, G. R., Pandey, R. N., Sahoo, R. N., Gupta, V. K., Datta, S. C., & Kumar, D. (2016). Monitoring nitrogen, phosphorus and sulphur in hybrid rice (*Oryza sativa* L.) using hyperspectral remote sensing. *Precision Agriculture*, *18*(5), 736–761. https://doi.org/10.1007/s11119-016-9485-2

McFeeters, S. (2013). Using the normalized difference water index (NDWI) within a geographic information system to detect swimming pools for mosquito abatement: A practical approach. *Remote Sensing*, *5*(7), 3544–3561. https://doi.org/10.3390/rs5073544

Onprasonk, S., Laohasiriwong, W., & Puttanapong, N. (2023). Spatial association between environmental factors and melioidosis in Thailand. *Research Square*. https://doi.org/10.21203/rs.3.rs-2961968/v1

Oukaltouma, K., El Moukhtari, A., Lahrizi, Y., Mouradi, M., Farissi, M., Willems, A., Qaddoury, A., Bekkaoui, F., & Ghoulam, C. (2020). Phosphorus deficiency enhances water deficit impact on some morphological and physiological traits in four faba bean (*Vicia faba* L.) varieties. *Italian Journal of Agronomy*, *16*(1), 1662. https://doi.org/10.4081/ija.2020.1662

Peng, S., Sanico, A. L., Garcia, F. V., Laza, R. C., Visperas, R. M., Descalsota, J. P., & Cassman, K. G. (2015). Effect of leaf phosphorus and potassium concentration on chlorophyll meter reading in rice. *Plant Production Science*, *2*(4), 227–231. https://doi.org/10.1626/pps.2.227

Peñuelas, J., Gamon, J. A., Fredeen, A. L., Merino, J., & Field, C. B. (1994). Reflectance indices associated with physiological changes in nitrogen- and water-limited sunflower leaves. *Remote Sensing of Environment*, *48*(2), 135–146. https://doi.org/10.1016/0034-4257(94)90136-8

Pimstein, A., Karnieli, A., Bansal, S. K., & Bonfil, D. J. (2011). Exploring remotely sensed technologies for monitoring wheat potassium and phosphorus using field spectroscopy. *Field Crops Research*, *121*(1), 125–135. https://doi.org/10.1016/j.fcr.2010.12.001

Pinter, P. J., Jr., Hatfield, J. L., Schepers, J. S., Barnes, E. M., Susan Moran, M., & Craig, S. T., & Daughtry, A. D. R. U. (2003). Remote Sensing for Crop Management. *Photogrammetric Engineering & Remote Sensing*, *69*(6), 647–664.

Qi, J., Chehbouni, A., Huete, A. R., Kerr, Y. H., & Sorooshian, S. (1994). A modified soil adjusted vegetation index. *Remote Sensing of Environment*, *48*(2), 119–126. https://doi.org/10.1016/0034-4257(94)90134-1

Rondeaux, G., Steven, M., & Baret, F. (1996). Optimization of soil-adjusted vegetation indices. *Remote Sensing of Environment*, *55*(2), 95–107. https://doi.org/10.1016/0034-4257(95)00186-7

Rouse, J. W., Haas, R. H., Schell, J. A., & Deering, D. W. (1973). Monitoring vegetation systems in the Great Plains with ERTS (earth resources technology satellite). In *Proceedings of 3rd earth resources technology satellite symposium* (pp. 309–317). National Aeronautics and Space Administration.

Rudoy, D., Garkusha, S., Skazhennik, M., Kiselev, E., Chizhikov, V., Petrushin, A., & Ignateva, S. (2020). Research of rice crops in Krasnodar region by remote sensing data. *E3S Web of Conferences*, *175*, 01004. https://doi.org/10.1051/e3sconf/202017501004

Ryu, J.-H., Jeong, H., & Cho, J. (2020). Performances of vegetation indices on paddy rice at elevated air temperature, heat stress, and herbicide damage. *Remote Sensing*, *12*(16), 2654. https://doi.org/10.3390/rs12162654

Saaty, T. L. (1977). A scaling method for priorities in hierarchical structures. *Journal of Mathematical Psychology*, *15*, 234–281. https://doi.org/10.1016/0022-2496(77)90033-5

Siedliska, A., Baranowski, P., Pastuszka-Woźniak, J., Zubik, M., & Krzyszczak, J. (2021). Identification of plant leaf phosphorus content at different growth stages based on hyperspectral reflectance. *BMC Plant Biology*, *21*(1), 28. https://doi.org/10.1186/s12870-020-02807-4

Singh, V., Pallaghy, C. K., & Singh, D. (2006). Phosphorus nutrition and tolerance of cotton to water stress. *Field Crops Research*, *96*(2–3), 199–206. https://doi.org/10.1016/j.fcr.2005.06.011

Sishodia, R. P., Ray, R. L., & Singh, S. K. (2020). Applications of remote sensing in precision agriculture: A review. *Remote Sensing*, *12*(19), 3136. https://doi.org/10.3390/rs12193136

Stein, B. R., Thomas, V. A., Lorentz, L. J., & Strahm, B. D. (2014). Predicting macronutrient concentrations from loblolly pine leaf reflectance across local and regional scales. *GIScience & Remote Sensing*, *51*(3), 269–287. https://doi.org/10.1080/15481603.2014.912875

Tairo, E. V., & Ndakidemi, P. A. (2013). *Bradyrhizobium japonicum* inoculation and phosphorus supplementation on growth and chlorophyll accumulation in soybean (*Glycine max* L.). *American Journal of Plant Sciences*, *04*(12), 2281–2289. https://doi.org/10.4236/ajps.2013.412282

Tisdale, S. L., & Nelson, W. L. (1985). *Soil fertility and fertilizers*. Macmillan Publishing Company.

Trigunasih, N. M., & Saifulloh, M. (2022). Correlation between soil nitrogen content and NDVI derived from Sentinel-2A satellite imagery. *Jurnal Lahan Suboptimal: Journal of Suboptimal Lands*, *11*(2), 112–119. https://doi.org/10.36706/jlso.11.2.2022.574

Velusamy, P., Rajendran, S., Mahendran, R. K., Naseer, S., Shafiq, M., & Choi, J.-G. (2021). Unmanned aerial vehicles (UAV) in precision agriculture: Applications and challenges. *Energies*, *15*(1), 217. https://doi.org/10.3390/en15010217

Wang, J., Zhou, Q., Shang, J., Liu, C., Zhuang, T., Ding, J., Xian, Y., Zhao, L., Wang, W., Zhou, G., Tan, C., & Huo, Z. (2021). UAV- and machine learning-based retrieval of wheat SPAD values at the over-wintering stage for variety screening. *Remote Sensing*, *13*(24), 5166. https://doi.org/10.3390/rs13245166

Xu, D., Liu, Y., Xu, W., & Guo, X. (2022). The impact of NPV on the spectral parameters in the yellow-edge, red-edge and NIR shoulder wavelength regions in grasslands. *Remote Sensing*, *14*(13), 3031. https://doi.org/10.3390/rs14133031

Xu, S., Xu, X., Blacker, C., Gaulton, R., Zhu, Q., Yang, M., Yang, G., Zhang, J., Yang, Y., Yang, M., Xue, H., Yang, X., & Chen, L. (2023). Estimation of leaf nitrogen content in rice using vegetation indices and feature variable optimization with information fusion of multiple-sensor images from UAV. *Remote Sensing*, *15*(3), 854. https://doi.org/10.3390/rs15030854

Yu, Y., Yu, H., Li, X., Zhang, L., & Sui, Y. (2023). Prediction of potassium content in rice leaves based on spectral features and random forests. *Agronomy*, *13*(9), 2337. https://doi.org/10.3390/agronomy13092337

Zhai, Y., Cui, L., Zhou, X., Gao, Y., Fei, T., & Gao, W. (2013). Estimation of nitrogen, phosphorus, and potassium contents in the leaves of different plants using laboratory-based visible and near-infrared reflectance spectroscopy: Comparison of partial least-square regression and support vector machine regression methods. *International Journal of Remote Sensing*, *34*(7), 2502–2518. https://doi.org/10.1080/01431161.2012.746484

Zhang, J., Cheng, T., Shi, L., Wang, W., Niu, Z., Guo, W., & Ma, X. (2022). Combining spectral and texture features of UAV hyperspectral images for leaf nitrogen content monitoring in winter wheat. *International Journal of Remote Sensing*, *43*(7), 2335–2356. https://doi.org/10.1080/01431161.2021.2019847

Zhang, S., Zhao, G., Lang, K., Su, B., Chen, X., Xi, X., & Zhang, H. (2019). Integrated satellite, unmanned aerial vehicle (UAV) and ground inversion of the SPAD of winter wheat in the reviving stage. *Sensors*, *19*(7), 1485. https://doi.org/10.3390/s19071485

Zhang, Y., Wang, T., Li, Z., Wang, T., & Cao, N. (2023). Based on machine learning algorithms for estimating leaf phosphorus concentration of rice using optimized spectral indices and continuous wavelet transform. *Frontiers in Plant Science*, *14*, 1185915. https://doi.org/10.3389/fpls.2023.1185915

Zhang, Z., Tang, B.-H., & Li, Z.-L. (2018). Retrieval of leaf water content from remotely sensed data using a vegetation index model constructed with shortwave infrared reflectances. *International Journal of Remote Sensing*, *40*(5–6), 2313–2323. https://doi.org/10.1080/01431161.2018.1471553

Zheng, H., Cheng, T., Li, D., Zhou, X., Yao, X., Tian, Y., Cao, W., & Zhu, Y. (2018). Evaluation of RGB, color-infrared and multispectral images acquired from unmanned aerial systems for the estimation of nitrogen accumulation in rice. *Remote Sensing*, *10*(6), 824. https://doi.org/10.3390/rs10060824

Zhou, J., Lu, X., Yang, R., Chen, H., Wang, Y., Zhang, Y., Huang, J., & Liu, F. (2022). Developing novel rice yield index using UAV remote sensing imagery fusion technology. *Drones*, *6*(6), 151. https://doi.org/10.3390/drones6060151

How to cite this article: Van Le, C., & Pham, L. T. (2025). Estimating leaf phosphorus concentration in rice by combining vegetation indices, texture features, and water indices from UAV multispectral imagery. *Agrosystems, Geosciences & Environment*, *8*, e70160. https://doi.org/10.1002/agg2.70160